

CALCIUM ABUNDANCE IN THE SOLAR WIND

P. WURZ AND P. BOCHSLER

Physics Institute, University of Bern, Sidlerstrasse 5, CH-3012 Bern, Switzerland;
peter.wurz@soho.unibe.ch, peter.bochsler@soho.unibe.ch

AND

J. A. PAQUETTE AND F. M. IPAVICH

University of Maryland-College Park, Space Physics, Building 224, Room 3203, College Park, MD 20742;
paquette@umtof.umd.edu, ipavich@umtof.umd.edu

Received 2002 July 8; accepted 2002 September 23

ABSTRACT

We report on the calcium abundance in the solar wind for an extended time period around the 1996 solar minimum. Data were recorded with the Mass Time-of-Flight (MTOF) sensor of the Charge, Element, and Isotope Analysis System (CELIAS) instrument on the *SOHO* spacecraft. The Ca/O abundance is 0.017 ± 0.003 for slow solar wind ($V_{\text{SW}} < 400 \text{ km s}^{-1}$) and 0.0053 ± 0.0014 for fast solar wind ($V_{\text{SW}} > 500 \text{ km s}^{-1}$). Compared to the photospheric Ca/O abundance ratio of $(\text{Ca}/\text{O})_{\text{PS}} = 0.00421 \pm 0.00079$, the solar wind clearly shows strong first ionization potential (FIP) fractionation as is expected for a low-FIP element. The Ca/H abundance is $A_{\text{Ca}} = 6.63 \pm 0.05$ and $A_{\text{Ca}} = 6.21 \pm 0.10$ for slow and fast solar winds, respectively. For comparison, the photospheric Ca abundance is $A_{\text{Ca}} = 6.36 \pm 0.02$.

Subject heading: solar wind

On-line material: color figures

1. INTRODUCTION

In this paper, we report on the investigation of the calcium density and abundance in the solar wind for a large velocity range. The data were gathered with the Mass Time-of-Flight sensor (MTOF) of the CELIAS instrument (Hovestadt et al. 1995) on the *Solar and Heliospheric Observatory (SOHO)* spacecraft. The *SOHO* spacecraft is located at the Lagrangian point L1 and is a three-axis stabilized platform pointing permanently at the Sun. Because of these unique observing conditions and the large active area of the MTOF sensor of the CELIAS instrument, measurements can be done with high time resolution and good statistics at the same time.

Calcium is an interesting element to study in the solar wind for at least two reasons. First, Ca is an element with a very low first ionization potential of 6.11 eV, which is considerably lower than the FIP of the commonly studied low-FIP elements Mg, Si, and Fe in the solar wind (see the review by von Steiger 1996). Second, Ca ions in the regular solar wind cannot be measured by the conventional linear time-of-flight (TOF) instruments (for example, SWICS-type sensors) since the small Ca signal is masked by the more abundant silicon and iron ions in the M–M/Q matrix. Since CELIAS/MTOF is an isochronous TOF spectrometer with high mass resolution, it has no problem resolving Ca ions in the recorded spectra. However, MTOF measures only the mass of the incoming ions and not their charge. Since our Charge TOF sensor (*SOHO/CELIAS/CTOF*) is also a linear TOF sensor, we do not anticipate being able to derive Ca abundances from CTOF data.

So far the Ca abundance in the solar wind has been determined mostly from solar energetic particles (SEPs) for the SEP-derived corona, for example, by Breneman & Stone (1985). Besides our earlier work in connection with the 1997 January 6 coronal mass ejection (CME) event (Wurz et al. 1997), there is one other study of the calcium abundance for slow solar wind in a limited velocity range (Kern et al.

1997). Thus, measuring the Ca abundance directly in the solar wind for a large solar wind velocity range should add to the general understanding of heavy ions in the solar wind.

2. DATA ANALYSIS

The CELIAS data processing unit accumulates TOF spectra every 5 minutes from the ions recorded with the MTOF sensor, which then are transmitted to Earth. The count rates for the mass peaks for the different elements were extracted from each of the transmitted TOF spectra by fitting the signal peak and the background using a maximum-likelihood method for Poisson statistics (Wurz 1999). Extraction of raw count rates of the Ca mass peaks from MTOF spectra is straightforward and is performed in the same way as was discussed before (Wurz et al. 1999). The raw count rates for the Ca peak are typically between 10 and 20 counts in a 5 minute spectrum, enough for reliable fitting of the mass line and background subtraction. In the spectra, the Ca peak is not contaminated by a doubly charged ion of higher mass, nor does the Ca signal suffer from being situated on the shoulder of a peak of a much more abundant element.

After the extraction of the raw counts, the overall efficiency of the MTOF sensor was calculated for each element and for each accumulation interval. To obtain particle fluxes for the chosen elements from the measured count rates, the MTOF sensor response comprising the transmission of the entrance system and the response of the isochronous TOF mass spectrometer (V-MASS) was taken into account (Wurz et al. 1999; Wurz 1999).

The actual solar wind plasma parameters, which were measured by the proton monitor (PM), a subunit of the MTOF sensor (Ipavich et al. 1998), are needed as input parameters for the calculation of the MTOF sensor response. The ionization state of Ca in the solar wind is not measured by MTOF. For slow solar wind in a limited

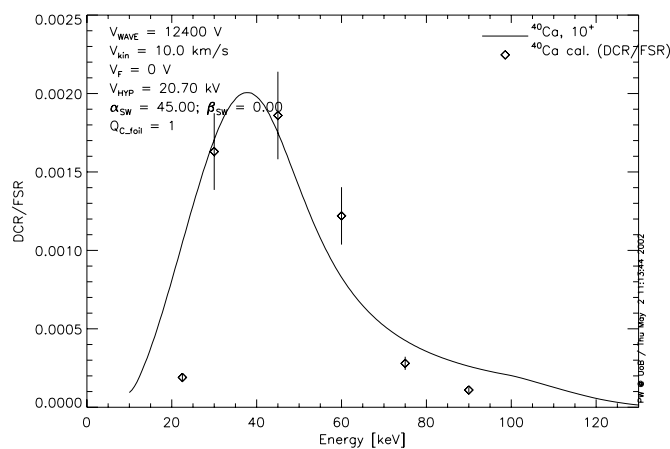


FIG. 1.—Calibration data from the MTOF flight-spares sensor for Ca (symbols) and the result of the instrument function (line). DCR/FSR stands for the double-coincidence rate vs. the start rate of the TOF section of the MTOF sensor.

velocity range, Ca was found to be mostly in the charge states 10^+ and 11^+ (Kern et al. 1997). Assuming ionization equilibrium in the solar corona (Arnaud & Rothenflug 1985), one finds that the Ca charge state distribution is quite stable for a large electron temperature range, which makes the data evaluation relatively simple and reliable. Nevertheless, since MTOF does not measure the ion charge, the actual charge-state distribution of the Ca ions in the solar wind during a measurement interval has to be derived from a simple model for the Ca freeze-in temperature using the proton plasma data (Wurz 1999). This model has been calibrated against in-flight charge-state data from CTOF and *Ulysses*/SWICS and data from other sources (Wurz et al. 1999; Wurz 1999).

The main difficulty in the data analysis is obtaining an absolute value for the Ca density in the absence of a preflight calibration of the MTOF sensor with calcium ions. The earlier results on the Ca abundance in the solar wind were derived without a calibration for Ca (Kern et al. 1997; Wurz et al. 1997). Recently, we performed calibrations with the MTOF flight-spares sensor, which is considered to be identical to the MTOF flight unit, in our calibration facility for solar wind plasma instrumentation (Marti et al. 2001). The result of this calibration is shown in Figure 1, where the measured ratio of the double coincidence to the start rate (DCR/FSR ratio) is plotted in comparison to the model instrument function. The DCR/FSR ratio basically represents the transmission of the time-of-flight section of the MTOF sensor. The agreement between the measured data and the model function is reasonable, considering the difficulty of the measurement. In addition to the limitations of the calibration data, deviations at the tails in the model function are caused by the actual angular and energy spread of the solar wind plasma being taken into account, whereas, in the calibration, a monoenergetic pencil beam has been used. We are planning to improve the measurements in future calibration campaigns.

3. RESULTS

An extended data set has been studied here to derive reliable average abundances of calcium in the solar wind. The data set evaluated for this study spans the time from day of

year (DOY) 30 through DOY 366 of 1996. Thus, the data set is representative of solar wind associated with the quiet Sun containing plasma associated with interstream solar wind and coronal hole solar wind. The latter arises from the equatorward extension of a polar coronal hole—the so-called Elephant Trunk’s coronal hole. No flares or CMEs that might interfere with the data analysis were observed in the particle data during this time period.

Figure 2 shows a section of the data used in the present study. The top two panels show the solar wind velocity and the proton density derived from PM measurements in order to give an impression of the state of the solar wind. The lower two panels give the solar wind calcium and iron densities derived from MTOF measurements. This is the first measurement of a time series of calcium densities in the solar wind. Individual measurements obtained from the MTOF sensor at each 5 minute measurement step are displayed in Figure 2, and no smoothing of the data has been performed. In general, the two heavy ion densities trace each other pretty well with time. However, the calcium density shows more noise than the iron density because its signal is lower by a factor of ~ 10 compared to the iron density. A meaningful temporal resolution for further scientific analysis in the heavy ion densities will be around an hour.

The variability in the heavy ion densities is much larger than the variability of the proton density. The He density and the heavy ion densities (O, Si, and Fe) generally show a much larger variation of their density than the protons (Neugebauer 1981; Wurz 1999); typically, the variation is larger by a factor of 10. This high variability we find is in good agreement with the known high variability of α particles with respect to protons in the solar wind. The α variability in the solar wind was reviewed by Neugebauer (1981), who found that the ratio of protons to α particles varies in the range from $n_p/n_\alpha = 8.1 \times 10^{-4}$ to 4.17×10^{-1} , a variation of a factor of 500. These short-term variations in the abundance are thought to be caused in the corona. With the available data, we are not able to distinguish between a temporal or a spatial nature, or both, of these variations. This high variability averages out when investigating longer time periods and causes hardly any systematic fractionation in the solar wind (Geiss et al. 1995). Our experience is that time periods exceeding a month are long enough to derive abundance data where the temporal/spatial variations average out (Wurz 1999; Wurz et al. 1999). We also find that the correlation between the heavy ion densities and the proton density is less pronounced than the correlation between the heavy ion densities themselves. However, occasionally even very brief features in the proton density are found in the heavy ion densities as well (see DOY 172 or DOY 210).

The results of the data analysis are given in Figure 3, which shows the calcium densities as a function of the solar wind velocity (the proton velocity) for the whole data set. The contours give the number of cases for a particular bin. The grouping of measurements at slow solar wind reflects that at solar minimum, mostly slow solar wind is observed in the ecliptic plane, with faster flows only during brief periods. The overlaid symbols in Figure 3 are the mean for a particular velocity bin and the error bars are the standard deviation of $\log(N_{Ca})$ for a single measurement. The large standard deviation basically reflects the large density fluctuations of Ca ions on short timescales. Such large density fluctuations on short timescales were observed earlier for Fe and Si ions in the solar wind (Aellig et al. 1999; Wurz et al.

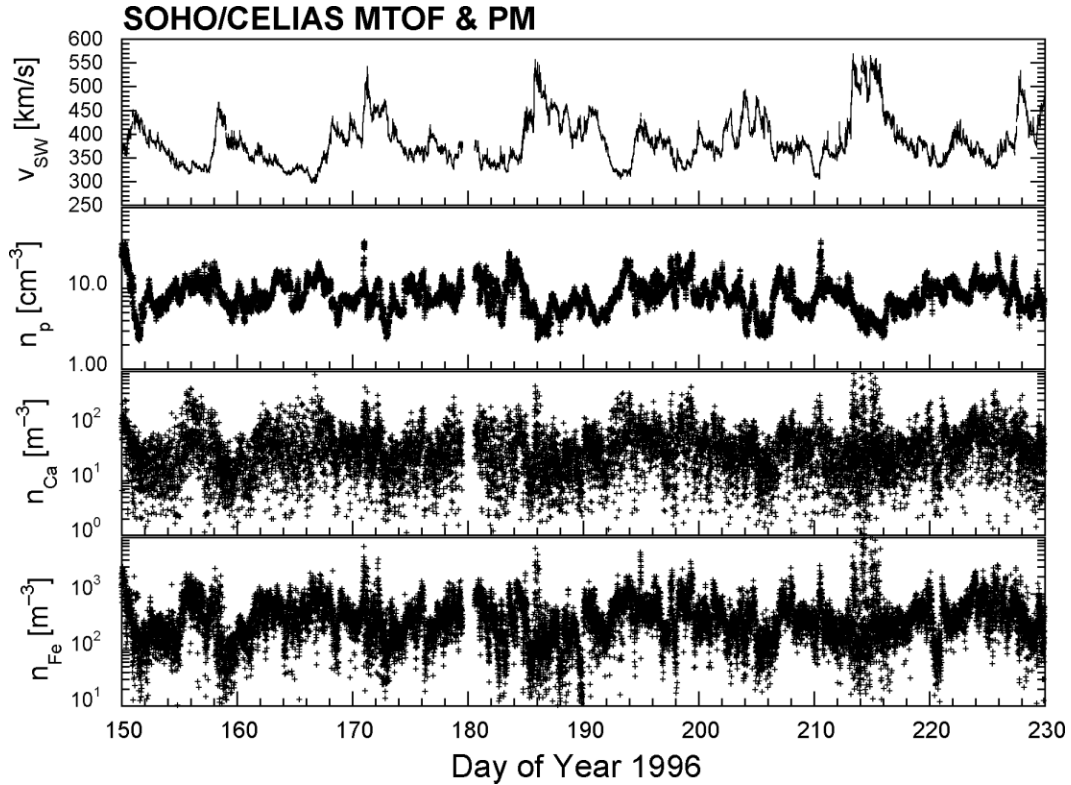


FIG. 2.—Period of 80 days of the data set used in this study, as derived from the MTOF and PM sensors of the *SOHO/CELIAS* instrument. Data are shown with a time resolution of 5 minutes. No smoothing has been applied to the data.

1999). What is immediately obvious from Figure 3 is that the Ca density decreases dramatically for solar wind speeds exceeding 450 km s^{-1} . Upon further data reduction, we derive the Ca density for slow, interstream-associated solar wind (i.e., $v_{\text{SW}} < 400 \text{ km s}^{-1}$) and fast, coronal hole-associated solar wind (i.e., $v_{\text{SW}} > 500 \text{ km s}^{-1}$). The values are $n_{\text{Ca}} = 41.1 \pm 4.3 \text{ m}^{-3}$ and $n_{\text{Ca}} = 5.7 \pm 1.8 \text{ m}^{-3}$, respectively. This decrease follows the same pattern as other heavy ions in the solar wind, e.g., the iron and silicon densities decrease with increasing solar wind speed by factors of about 3 and 5, respectively (Wurz et al. 1999). Even the oxygen density drops, which serves as a reference in many investigations concerning the abundance of heavy ions in the solar wind, but only by a factor of less than 2 (Wurz 1999).

For many heavy ion abundance studies in the solar wind, the abundance ratio with respect to oxygen has been used. The Ca/O abundance ratio is shown in Figure 4 in the same format as was used in Figure 3. We find that the Ca/O ratio is roughly constant for slow solar wind ($v_{\text{SW}} < 400 \text{ km s}^{-1}$) and for fast solar wind ($v_{\text{SW}} > 500 \text{ km s}^{-1}$). Unlike our earlier Si and Fe observations, in which we observed a smooth transition over a wide velocity range between the slow and fast solar wind regimes (Aellig et al. 1999; Wurz et al. 1999), the transition for the Ca/O abundance ratio is more abrupt. We speculate that Ca reacts faster to changes in the solar atmosphere than Fe or Si since it ionizes faster, i.e., farther down in the solar atmosphere. Upon further data reduction, we get $n_{\text{Ca}}/n_{\text{O}} = 0.017 \pm 0.003$ and $n_{\text{Ca}}/n_{\text{O}} = 0.0053 \pm 0.0014$ for slow and fast solar winds, respectively. The difference in these two ratios reflects the different FIP fractionation in slow and fast solar winds.

4. DISCUSSION

The aim of this study was to derive the calcium abundance in the slow and fast solar wind with good statistics in a manner similar to that used for the silicon and iron ions before (Wurz et al. 1999). Furthermore, we wanted to compare the Ca abundance with other measurements and with the photosphere in particular.

When solar wind abundance data are presented in the usual way for solar wind research that is relative to oxygen, the calcium abundance ratio for slow solar wind comes out to be significantly higher than for fast solar wind. This observation is known as FIP fractionation for low-FIP elements. From the present data analysis, we derive an FIP fractionation factor, i.e., the elemental abundance ratio in the solar wind (SW) with respect to the elemental abundance ratio in the photosphere (PS) from

$$f_{\text{Ca/O}} = \frac{(\text{Ca/O})_{\text{SW}}}{(\text{Ca/O})_{\text{PS}}} . \quad (1)$$

We calculate the photospheric Ca/O abundance ratio from optical measurements in the photosphere. While the photospheric Ca abundance seems to be settled in the literature at a value of $A_{\text{Ca}} = 6.36 \pm 0.02$ (Anders & Grevesse 1989; Grevesse & Anders 1991; Grevesse & Sauval 1998), the O abundance was revised a few times recently. In their well-known survey, Anders & Grevesse (1989) reported $A_{\text{O}} = 8.93 \pm 0.035$; later, Grevesse & Noels (1993) reported $A_{\text{O}} = 8.87 \pm 0.07$ and Grevesse & Sauval (1998) reported $A_{\text{O}} = 8.83 \pm 0.06$. Most recently, Holweger (2001) reported $A_{\text{O}} = 8.736 \pm 0.078$ together with a detailed discussion regarding the causes of the different oxygen abundances

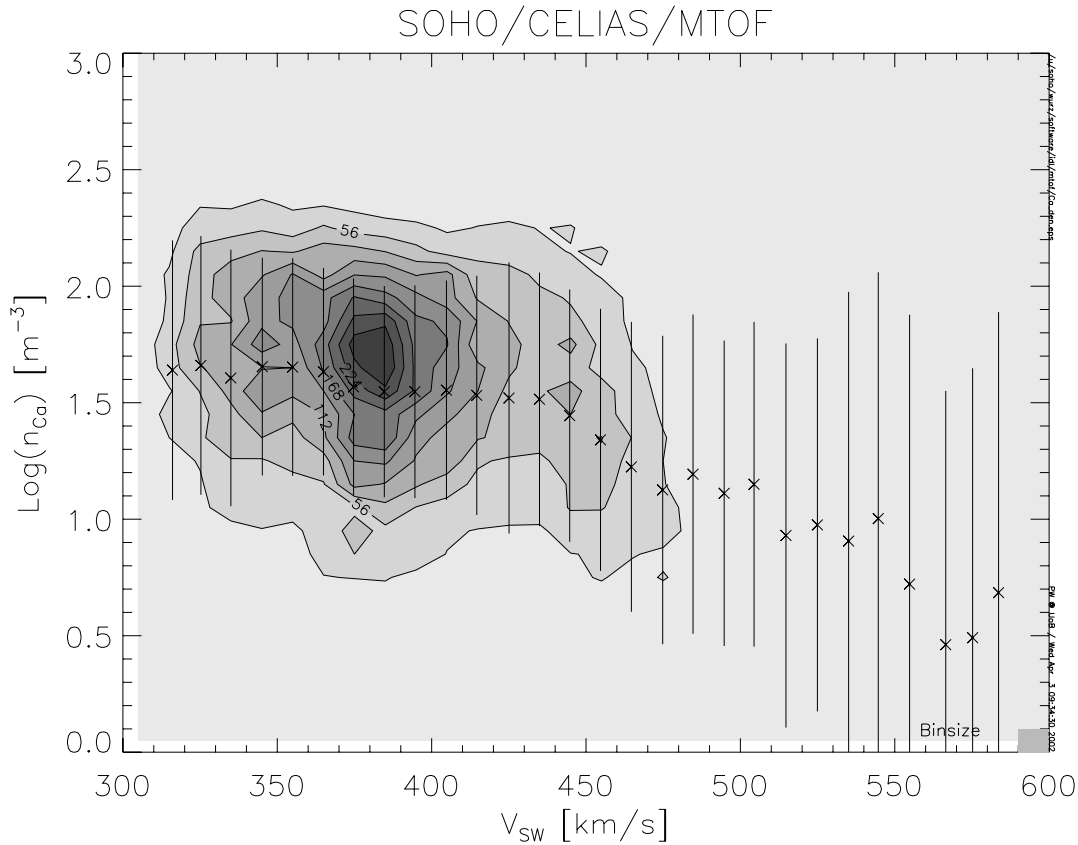


FIG. 3.—Logarithm of calcium densities measured with CELIAS/MTOF at 1 AU vs. the solar wind velocity. *Ten linearly spaced contours:* Number of measurements for a particular bin. Data have been selected from DOY 30 through DOY 366 of 1996. During that time period, there was mostly slow solar wind, which explains the clustering of measurements between 300 and 400 km s⁻¹. *Crosses:* Mean for a particular velocity bin. *Error bars:* Standard deviation of log(N_{Ca}) for a single measurement. [See the electronic edition of the Journal for a color version of this figure.]

in these studies. We adopt the latest value for the oxygen abundance and get for the photospheric ratio $(Ca/O)_{PS} = (4.21 \pm 0.79) \times 10^{-3}$. Using that number, we get FIP fractionations $f_{Ca/O} = 4.04 \pm 1.04$ and $f_{Ca/O} = 1.26 \pm 0.41$ for slow and fast solar winds, respectively. The difference in FIP fractionation for slow and fast solar winds is typical for a low-FIP element (Geiss et al. 1995; von Steiger 1996). Earlier, we found a similar FIP step for silicon and a smaller step for iron (Wurz et al. 1999). Our FIP fractionation factors compare well with recent optical observations performed with the SUMER on board *SOHO* (Feldman et al. 1998). The authors find for the corona along the equatorial plane, $f_{Ca/O} = 4.1$, and for a coronal hole above the south pole, $f_{Ca/O} = 1.1$ (from their Figs. 4 and 5, respectively).

Although the solar wind speed rarely exceeded 600 km s⁻¹ during the investigated time interval, we can associate this solar wind speed regime with flow from coronal holes extending toward the solar equator (e.g., the well-known Elephant Trunk coronal hole during summer 1996) since the Ca/O abundance ratio saturates at a low level, consistent with the present knowledge of FIP fractionation for low-FIP elements. It has been clear for some time that there is a correlation between the size of the coronal hole on the solar surface and the maximum solar wind speed (Nolte et al. 1976), with minimum speeds of coronal hole solar wind of 425 km s⁻¹. Very fast solar wind flow (about 800 km s⁻¹) that obviously originates from the large polar coronal holes has only been observed out of the ecliptic during the 1996 time period (McComas et al. 2000).

Similar results for the elemental fractionation are obtained when using hydrogen as the reference instead of oxygen. We find a Ca/H abundance ratio of $(4.28 \pm 0.49) \times 10^{-6}$ and $(1.61 \pm 0.38) \times 10^{-6}$ for slow and fast solar winds, respectively. The Ca/H abundance ratios were obtained in the same way as the Ca/O ratios, with the exception that the proton data were taken from the PM. We added these Ca/H ratios to the compilation of data given in Table 1. Hydrogen apparently behaves like a high-FIP element, as was concluded earlier by Meyer (1993).

In order to compare our Ca abundance with other measurements, we conducted a search of known measurements of the solar calcium abundance in various regimes. This compilation of data is shown in Table 1 together with the solar wind results reported in this study. Abundance data from the photosphere, the solar corona, SEPs, and solar flares are given. If not measured directly, we tried to derive from the reported measurements a Ca/H abundance ratio and a calcium density in the solar wind at 1 AU using certain assumptions that are detailed in Table 1. The survey of Ca/H abundance ratio data is shown in Figure 5. From optical measurements, it appears that the solar corona has a somewhat elevated Ca/H abundance ratio compared to the photosphere. Using the photospheric calcium abundance (Grevesse & Sauval 1998), we would expect a calcium density in the solar wind of about 23 m⁻³ at 1 AU. Using the solar corona measurement from Veck & Parkinson (1981), the expected calcium density is about 32 ± 12 m⁻³ at 1 AU. The calcium density in

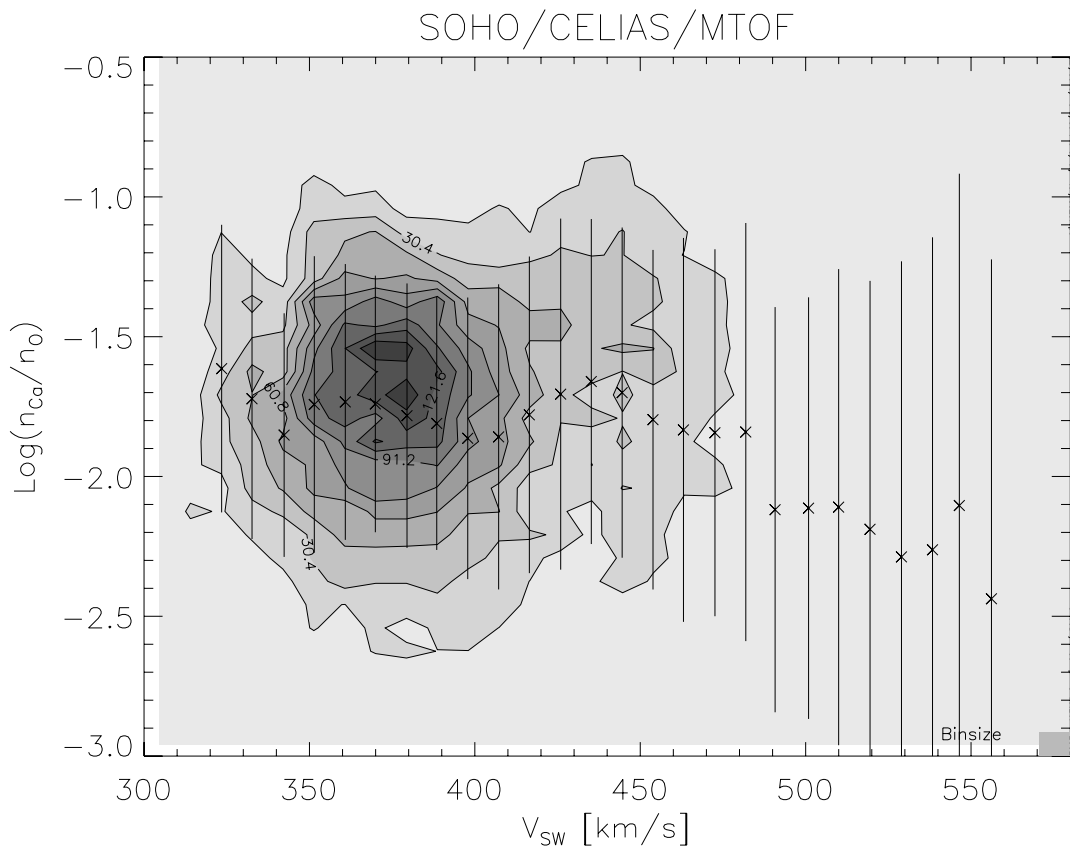


FIG. 4.—Logarithm of calcium to oxygen abundance ratio measured with CELIAS/MTOF at 1 AU vs. the solar wind velocity. *Ten linearly spaced contours:* Number of measurements for a particular bin. Data have been selected from DOY 30 through DOY 366 of 1996. During that time period, there was mostly slow solar wind, which explains the clustering of measurements between 300 and 400 km s⁻¹. *Crosses:* Mean for a particular velocity bin. *Error bars:* Standard deviation of log(N_{Ca}/N_O) for a single measurement. [See the electronic edition of the Journal for a color version of this figure.]

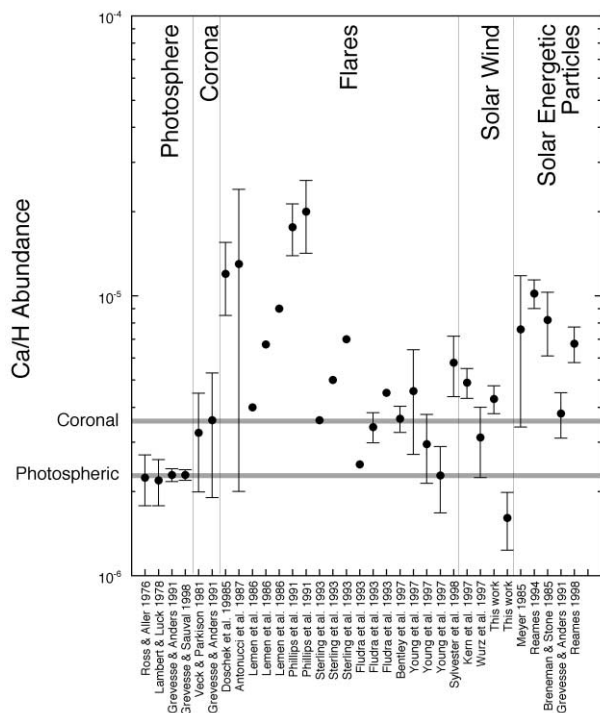


FIG. 5.—Summary of published Ca abundance measurements. *Lower gray line:* Photospheric Ca abundance. *Upper gray line:* Coronal Ca abundance. See text and Table 1 for details.

the solar wind derived in this work is $41.1 \pm 4.3 \text{ m}^{-3}$ for a solar wind velocity range from 300 to 400 km s⁻¹. Comparing the Ca/H abundance data with our solar wind measurements, it appears that calcium is enriched in the slow interstream-associated solar wind and depleted in the fast coronal hole solar wind.

Calcium abundance ratios, with respect to hydrogen derived from measurements of flares and SEPs, show a large variation from event to event. Several groups report minimum, average, and maximum abundance ratios (Fludra et al. 1993; Lemen, Sylvester, & Bentley 1986; Sterling, Doschek, & Feldman 1993) that we reproduced in Table 1 and Figure 5. Flares even show considerable variations in their elemental composition during the event itself (Veck & Parkinson 1981). This makes SEPs and flares unreliable candidates for the determination of the photospheric composition or regular solar wind composition. With some assumptions, one can remove the mass bias in the composition of SEPs to derive a so-called baseline composition of the SEPs that is assumed to be representative for the elemental abundances in the solar corona (Breneman & Stone 1985; Meyer 1985). This, indeed, seems to be the case. If for the Ca/Si abundance ratios in SEPs the solar wind density of silicon is used (Wurz 1999; Wurz et al. 1999), the Ca densities obtained from SEPs agree with the solar coronal value from Veck & Parkinson (1981) quite well, and we take it as coronal abundance despite its large uncertainty. The calcium in the slow solar wind appears to reflect the coronal abundance as well.

TABLE 1
CALCIUM ABUNDANCE DATA

Measured Regime	Measured Quantity	Method	Measured Value	Ca/H Derived	Ca Density (m ⁻³)	Reference
Photosphere.....	Ca/H	Optical	(2.24 ± 0.46) × 10 ⁻⁶	...	22.4 ^a	1
Photosphere.....	Ca/H	Optical	(2.19 ± 0.41) × 10 ⁻⁶	...	21.9 ^a	2
Photosphere.....	Ca/H	Optical	(2.29 ± 0.12) × 10 ⁻⁶	...	22.9 ^a	3
Photosphere.....	Ca/H	Optical	(2.29 ± 0.10) × 10 ⁻⁶	...	22.9 ^a	4
Solar corona	Ca/H	Optical	3.24 ^{+1.33} _{-1.23} × 10 ⁻⁶	...	32.4 ^a	5
Solar corona	Ca/H	Optical	Min. 4 × 10 ⁻⁶ , Avg. 6.7 × 10 ⁻⁶ , Max. 9 × 10 ⁻⁶	...	67 ^a	6
Solar flare	Ca/Fe	Optical	0.10 ± 0.015	1.2 ^{+0.31} _{-0.38} × 10 ⁻⁵ ^d	31.6 ^e	7
Solar flare	Ar/Ca	Optical	0.20 ± 0.20	(1.3 ± 1.3) × 10 ⁻⁵ ^g	130 ^a	8
Solar flare	Fe/Ca	Optical	6.8 ± 1.0, 6.0 ± 1.5	(1.76 ± 0.37) × 10 ⁻⁵ ^d , (2.00 ± 0.58) × 10 ⁻⁵ ^d	46.5 ^e , 52.7 ^e	9
Solar flare	Ca/H	Optical	Min. 3.6 × 10 ⁻⁶ , Avg. 5.0 × 10 ⁻⁶ , Max. 7.0 × 10 ⁻⁶	...	50 ^a	10
Solar flare	Ca/H	Optical	Min. 2.5 × 10 ⁻⁶ , Avg. (3.40 ± 0.42) × 10 ⁻⁶ , Max. 4.5 × 10 ⁻⁶	...	34 ^a	11
Solar flare	Ca/H	Optical	(3.64 ± 0.39) × 10 ⁻⁶	...	36.4 ^a	12
Solar flare	Ar/Ca	Optical	0.55 ± 0.21, 0.85 ± 0.21, 1.10 ± 0.25	(4.57 ± 1.86) × 10 ⁻⁶ ^g , (2.95 ± 0.81) × 10 ⁻⁶ ^g , (2.28 ± 0.61) × 10 ⁻⁶ ^g	29.5 ^a	13
Solar flare	Ca/H	Optical	(5.77 ± 1.41) × 10 ⁻⁶	...	58 ^a	14
Solar wind, slow.....	Ca/Si	Particles	0.049 ± 0.006	(4.9 ± 0.8) × 10 ⁻⁶ ^e	19.5 ^b	15
Solar wind, slow.....	Ca/O	Particles	0.0134 ± 0.0032	(3.12 ± 0.88) × 10 ⁻⁶ ^e	29	16
Solar wind, fast	Ca/O	Particles	0.0186 ± 0.0042	(5.0 ± 0.15) × 10 ⁻⁶ ^e	35	16
Solar wind, slow.....	Ca/O	Particles	0.017 ± 0.003	This work
Solar wind, slow.....	Ca/O	Particles	0.0053 ± 0.0014	This work
Solar wind, slow.....	n[Ca]	Particles	41.1 ± 4.3 m ⁻³	(4.28 ± 0.49) × 10 ⁻⁶ ^f	41.1 ± 4.3	This work
Solar wind, fast	n[Ca]	Particles	5.7 ± 1.8 m ⁻³	(1.61 ± 0.38) × 10 ⁻⁶ ^f	5.7 ± 1.8	This work
SEP, mass unbiased baseline	Ca/Si	Particles	0.076 ± 0.042	(7.6 ± 4.2) × 10 ⁻⁶ ^e	30.2 ^b	17
SEP-derived corona	Ca/Si	Particles	0.082 ^{+0.014} _{-0.012}	8.2 ^{+2.2} _{-2.0} × 10 ⁻⁶ ^e	32.6 ^b	18
SEP.....	Ca/Si	Particles	0.077 ± 0.01	(1.02 ± 0.12) × 10 ⁻⁵	30.6 ^b	19
SEP-derived corona	Ca/H	Particles	(3.80 ± 0.70) × 10 ⁻⁶	...	38 ^a	3
SEP-derived corona	Ca/O	Particles	(10.6 ± 0.4) × 10 ⁻³	(6.75 ± 0.98) × 10 ⁻⁶ ^e	67.5 ^a	20

NOTE.—Calcium abundance data in the photosphere, in the solar corona, in SEPs, and in solar flares are given together with our solar wind data. From the reported measurements, calcium abundance in the solar wind and the density at 1 AU is derived using assumptions given below.

^a Value is derived by assuming a proton density of 10 cm⁻³ at 1 AU.

^b Value is derived using a Si density of 400 m⁻³ at 1 AU; Wurz et al. 1999; Wurz 1999.

^c Value is derived using a Fe density of 316 m⁻³ at 1 AU; Wurz et al. 1999; Wurz 1999.

^d Value is derived using Fe/H = 1.2 × 10⁻⁴ from Ipavich et al. 1986.

^e Value is derived using the Si/O abundance of 0.19 from Bochsler 1989 and the H/O abundance of 1900 from Bame et al. 1975.

^f The proton density was measured with the Proton Monitor, a subsensor of CELIAS/MTOF.

^g Value is derived using an argon abundance of A_{Ar} = 6.40 ± 0.06; Grevesse & Sauval 1998.

REFERENCES.—(1) Ross & Aller 1976; (2) Lambert & Luck 1978; (3) Grevesse & Anders 1991; (4) Grevesse & Sauval 1998; (5) Veck & Parkinson 1981; (6) Lemen et al. 1986; (7) Doschek et al. 1985; (8) Antonucci et al. 1987; (9) Phillips & Feldman 1991; (10) Sterling et al. 1993; (11) Fludra et al. 1993; (12) Bentley, Sylvester, & Lemen 1997; (13) Young et al. 1999a; (14) Sylvester et al. 1998; (15) Kern et al. 1997; (16) Wurz et al. 1997; (17) Meyer 1985; (18) Breneman & Stone 1985; (19) Reames 1994; (20) Reames 1998.

Fludra et al. (1993) determined the abundances of S, Ca, and Fe relative to hydrogen for several flares. The authors also performed detailed analysis of the abundance ratios with respect to the temperature of the flare at the time when the spectra were taken. The abundance ratios S/H and Fe/H showed a strong dependence on the flare temperature, whereas the Ca/H abundance ratio was almost independent of the electron temperature. This finding suggests that calcium is ionized far down in the solar atmosphere before the flare acceleration takes place.

A few years ago, Feldman (1992) and later Falconer, Davila, & Thomas (1997) introduced the class of very low-FIP elements with an FIP lower than 6.1 eV to dis-

tinguish these elements from low-FIP elements with an FIP from 7.5 to 10 eV. This new category was introduced on the basis of behavioral differences from the other low-FIP elements. From our measurements, we cannot support such a distinction. The very low-FIP elements Ca and Al (Bochsler et al. 2000) behave in the same manner as the well-studied low-FIP elements Si and Fe (Aellig et al. 1999; Wurz et al. 1999). In a recent review, Feldman & Lamming (2000) concluded, primarily on the basis of optical flare observations, that the present spectroscopic data is not sufficient to decide conclusively whether or not there is a different fractionation factor for elements with very low FIP.

5. CONCLUSIONS

In this study, we were able to derive the local Ca density at the location of the *SOHO* spacecraft (≈ 1 AU) and the abundance ratios Ca/O and Ca/H. We find the following:

1. A Ca/O abundance ratio of 0.017 ± 0.003 and 0.0053 ± 0.0014 for slow and fast solar winds, respectively. For comparison, the photospheric Ca/O abundance ratio is $(\text{Ca/O})_{\text{PS}} = 0.00421 \pm 0.00079$.

2. A Ca/H abundance of $A_{\text{Ca}} = 6.63 \pm 0.05$ and $A_{\text{Ca}} = 6.21 \pm 0.10$ for slow and fast solar winds, respectively. For comparison, the photospheric Ca abundance is $A_{\text{Ca}} = 6.36 \pm 0.02$.

3. A Ca density of $41.1 \pm 5.3 \text{ m}^{-3}$ for slow solar wind ($V_{\text{SW}} < 400 \text{ km s}^{-1}$) and $5.7 \pm 1.8 \text{ m}^{-3}$ for fast solar wind ($V_{\text{SW}} > 500 \text{ km s}^{-1}$).

4. FIP fractionations $f_{\text{Ca/O}} = 4.04 \pm 1.04$ and $f_{\text{Ca/O}} = 1.26 \pm 0.41$ for slow and fast solar winds, respectively. Thus, calcium shows the same fractionation behavior as other low-FIP elements with respect to different solar wind regimes.

Note that all quoted errors are 1σ values. From our survey of published Ca/H abundance ratios and the comparison with our solar wind values (Table 1 and Fig. 5), we conclude that Ca is enriched in the slow solar wind compared to its photospheric abundance. Oxygen, a high-FIP element, must be depleted since the FIP step is almost a factor of 2 larger than the coronal enrichment of the Ca abundance. For the fast solar wind, both Ca and O appear to be depleted compared to their photospheric abundances. How-

ever, considering the error bars of the photospheric Ca abundance and the Ca abundance in the fast solar wind we observed (see Table 1), we find that at the extremes of these errors, the two values are very close. Our conclusions on enrichments or depletions of elements in the solar wind compared to the photosphere are based on comparisons of abundance ratios using hydrogen as a reference. In a large review, Meyer (1993) concluded that high-FIP elements have photospheric abundances with respect to H, while low-FIP elements are enhanced using abundance data from in SEPs, the solar wind, and EUV and X-ray spectroscopy. Hydrogen behaves like the heavier high-FIP elements, which means that a larger Ca/H ratio in the corona and in the solar wind results from a depletion of H and not from an enrichment of Ca.

The authors gratefully acknowledge the assistance of S. E. Lasley from the University of Maryland and M. Hohl from the University of Bern during the MTOF flight-spares calibration campaign. This work is supported by the Swiss National Science Foundation. CELIAS is a joint effort of five hardware institutions under the direction of the Max-Planck Institut für Extraterrestrische Physik (prelaunch) and the University of Bern (post-launch). The Max-Planck Institut für Aeronomie was the prime hardware institution for CTOF, the University of Maryland was the prime hardware institution for MTOF, the University of Bern provided the entrance systems for both sensors, and the Technical University of Braunschweig provided the DPU.

REFERENCES

- Aellig, M. R., Hefti, S., Grünwaldt, H., Bochsler, P., Wurz, P., Ipavich, F. M., & Hovestadt, D. 1999, *J. Geophys. Res.*, 104, 24769
- Anders, E., & Grevesse, N. 1989, *Geochim. Cosmochim. Acta*, 53, 197
- Antonucci, E., Marocchi, D., Gabriel, A. H., & Doschek, G. A. 1987, *A&A*, 188, 159
- Arnaud, M., & Rothenflug, R. 1985, *A&AS*, 60, 425
- Bame, S. J., Asbridge, J. R., Feldman, W. C., Montgomery, M. D., & Kearney, P. D. 1975, *Sol. Phys.*, 43, 463
- Bentley, R. D., Sylvester, J., & Lemen, J. R. 1997, *Adv. Space Res.*, 20, 2275
- Bochsler, P. 1989, *J. Geophys. Res.*, 94, 2365
- Bochsler, P., Ipavich, F. M., Paquette, J. A., Weygand, J. M., & Wurz, P. 2000, *J. Geophys. Res.*, 105, 12659
- Breneman, H. H., & Stone, E. C. 1985, *ApJ*, 299, L57
- Doschek, G. A., Feldman, U., & Seely, J. F. 1985, *MNRAS*, 217, 317
- Falconer, D. A., Davila, J. M., & Thomas, R. J. 1997, *ApJ*, 482, 1050
- Feldman, U. 1992, *Phys. Scripta*, 46, 202
- Feldman, U., & Laming, J. M. 2000, *Phys. Scripta*, 61, 222
- Feldman, U., Schüle, U., Widing, K. G., & Laming, J. M. 1998, *ApJ*, 505, 999
- Fludra, A., Culhane, J. L., Bentley, R. D., Doschek, G. A., Hiei, E., Phillips, K. J. H., Sterling, A., & Watanabe, T. 1993, *Adv. Space Res.*, 13, 395
- Geiss, J., Gloeckler, G., & von Steiger, R. 1995, *Space Sci. Rev.*, 72, 49
- Grevesse, N., & Anders, E. 1991, in *Solar Interior and Atmosphere*, ed. A. N. Cox, W. C. Livingston, & M. S. Matthews (Tucson: Univ. Arizona Press), 1227
- Grevesse, N., & Noels, A. 1993, in *Origin and Evolution of Elements*, ed. N. Prantzos, E. Vangioni-Flam, & M. Cassé (Cambridge: Cambridge Univ. Press), 15
- Grevesse, N., & Sauval, A. J. 1998, *Space Sci. Rev.*, 85, 161
- Holwegger, H. 2001, in *AIP Conf. Proc. 598, Solar and Galactic Composition*, ed. R. F. Wimmer-Schweingruber (Berlin: Springer), 23
- Hovestadt, D., et al. 1995, *Sol. Phys.*, 162, 441
- Ipavich, F. M., et al. 1986, *J. Geophys. Res.*, 91, 4133
- . 1998, *J. Geophys. Res.*, 103, 17205
- Kern, O., Wimmer-Schweingruber, R. F., Bochsler, P., Gloeckler, G., & Hamilton, D. C. 1997, *ESA Science Publications*, ed. B. Fleck & A. Wilson (ESA SP-415; Noordwijk: ESA), 345
- Lambert, D. L., & Luck, R. E. 1978, *MNRAS*, 183, 79
- Lemen, J. R., Sylvester, J., & Bentley, R. D. 1986, *Adv. Space Res.*, 6, 245
- Marti, A., Schletti, R., Wurz, P., & Bochsler, P. 2001, *Rev. Sci. Instrum.*, 72, 1354
- McComas, D. J., et al. 2000, *J. Geophys. Res.*, 105, 10419
- Meyer, J.-P. 1985, *ApJS*, 57, 151
- . 1993, in *Origin and Evolution of Elements*, ed. N. Prantzos, E. Vangioni-Flam, & M. Cassé (Cambridge: Cambridge Univ. Press), 26
- Neugebauer, M. 1981, in *Fundamentals of Cosmic Physics*, Vol. 7, (London: Gordon & Breach), 131
- Nolte, J. T., et al. 1976, *Sol. Phys.*, 46, 303
- Phillips, K. J. H., & Feldman, U. 1991, *ApJ*, 379, 401
- Reames, D. V. 1994, *Adv. Space Res.*, 14, 177
- . 1998, *Space Sci. Rev.*, 85, 327
- Ross, J. E., & Aller, J. H. 1976, *Science*, 191, 1223
- Sterling, A. C., Doschek, G. A., & Feldman, U. 1993, *ApJ*, 404, 394
- Sylvester, J., Lemen, J. R., Bentley, R. D., Fludra, A., & Zolcinski, M.-C. 1998, *ApJ*, 501, 397
- Veck, N. J., & Parkinson, J. H. 1981, *MNRAS*, 197, 41
- von Steiger, R. 1996, in *Solar Wind Eight*, ed. D. Winterhalter, J. T. Gosling, S. R. Habbal, W. S. Kurth, & M. Neugebauer (College Park: AIP), 193
- Wurz, P., et al. 1997, *ESA Science Publications*, B. Fleck & A. Wilson, (ESA SP-415; Noordwijk: ESA), 395
- Wurz, P. 1999, *Habilitation thesis*, Univ. Bern, Switzerland
- Wurz, P., et al. 1999, *Phys. Chem. Earth (C)*, 24, 421
- Young, P. R., Mason, H. E., Keenan, F. P., & Widing, K. G. 1997, *A&A*, 323, 243